Real-time, local basis-set implementation of time-dependent density functional theory for excited state dynamics simulations

Sheng Meng[a] and Efthimios Kaxiras
Department of Physics and School of Engineering and Applied Sciences, Harvard University, Cambridge, Massachusetts 02138, USA

(Received 21 April 2008; accepted 26 June 2008; published online 5 August 2008)

We present a method suitable for large-scale accurate simulations of excited state dynamics within the framework of time-dependent density functional theory (DFT). This is achieved by employing a local atomic basis-set representation and real-time propagation of excited state wave functions. We implement the method within SIESTA, a standard ground-state DFT package with local atomic basis, and demonstrate its potential for realistic and accurate excited state dynamics simulations using small and medium-sized molecules as examples (H_2, CO, O_3, and indolequinone). The method can be readily applied to problems involving nanostructures and large biomolecules. © *2008 American Institute of Physics*. [DOI: 10.1063/1.2960628]

I. INTRODUCTION

Excited electronic states are quite common in nature, encountered, for example, in processes such as ignition, respiration, light absorption, and fluorescence. Many experimental probes rely on activating the system to excited states for detection, as in optical spectroscopy, pump-probe laser spectroscopy, photoelectron emission, and scanning tunneling microscopy. Accordingly, an accurate treatment of excited electronic states and the related dynamical processes is crucial for the fundamental understanding of many natural processes, as well as for interpreting a vast amount of experimental data collected through probes that involve electron excitation. A full description of excited states at the atomic (molecular vibration) and electronic (absorption and emission) levels, and especially coupled ion-electron motion under strong fields, represents great computational challenges because of the difficulties in describing excited state wave functions accurately and due to large demands on computational resources.

Density functional theory (DFT) based on the single-particle Kohn–Sham (KS) equations,[1] has proven successful in describing ground-state properties, such as bond lengths and bond energies, but is not suitable for treating excited states quantitatively. A well-known example is the inability of DFT to reproduce the semiconductor band gaps which are usually underestimated by more than 50% compared to experimental values. This failure is attributed to the lack of electron-hole interactions and the screening effects in DFT.

Time-dependent DFT (TDDFT) developed for a generic time-dependent potential by Runge and Gross,[2] can give accurate values for band gaps, absorption peak positions, and polarizabilities within the linear response regime, as well as many other excited state properties including potential energy surfaces, nonadiabatic couplings, molecular vibrations under a strong field, electron transport, and atom collisions.[3] Although an exact theory in principle, TDDFT in its current incarnation based on the adiabatic local density approximation (ALDA) has limitations when dealing with Rydberg states, charge transfer, and multiple excitation states.[4,5] However, incorporating exact-exchange or modified algorithms in the exchange-correlation functional shows significant improvements for excitation energies in these challenging situations, with the possible exception of multiple excitations.[6–9] It is suitable for simulations of excited state dynamics, while maintaining the computational efficiency of DFT, such as computational speed and high accuracy.

There are a number of numerical implementations of TDDFT. Most conventional TDDFT calculations involve the linear response to an external field with a given frequency, and are usually formulated in the frequency domain.[10,11] These schemes can reproduce absorption spectra and oscillator strengths accurately by calculating the poles of the density-density response function; however, they have problems related to linear response itself and the choice of exchange-correlation functions. Real-time propagation of wave functions, namely, calculating TDDFT in the time domain, can partly solve the problem related to linear response because it does not rely on perturbation theory so it could include nonlinear effects. Real-time TDDFT was first implemented by Theilhaver,[12] followed by important developments of Yabana and Bertsch[13] and Yabana *et al.*,[14] and has become the focus of the OCTUPUS code.[15] Among recent implementations, different basis sets have been used, typically based on plane waves,[16–19] Gaussian functions,[20] or real-space grids.[15,21,22] These approaches are either computationally very demanding, especially for finite systems which involve a large vacuum region, or less efficient for systems with abrupt electron density changes such as embedded transition metals in biomolecules.

Here we propose to use local atomic basis sets and real-time propagation of wave functions for solving the time-dependent KS (TDKS) equations. This approach has several advantages.

[a]Electronic mail: shmeng@deas.harvard.edu.

(i) Within the real-time TDDFT approach, nonlinear effects and strong electric fields can be applied, which is useful for understanding many physical processes, for example, laser manipulation of molecules.
(ii) Real-time simulations reveal directly the information about the ultrafast dynamics of electrons and ions upon excitation, which dominates in photochemical reactions and ultrafast laser spectroscopy.
(iii) The use of local basis sets reduces significantly the number of basis functions used to represent the electronic wave functions while maintaining relatively high accuracy, thus enabling us to simulate systems of larger size with a small memory requirement and a short computing time.
(iv) The scheme can be easily parallelized because the occupied (after excitation) molecular orbitals are propagated independently at a time, and can be distributed evenly over several processors with little mutual communication.
(v) The local basis functions, which are exactly zero outside a sphere of certain diameter around the ions, lead to a linear scaling (order-N) of the algorithm with respect to the number of electrons N, enabling simulations of large systems.
(vi) Within the same scheme, quantities such as absorption spectra and polarizability can also be calculated readily.[23,24]

These are important advantages, particularly in what concerns simulations of excited state dynamics of biomolecules.

The above procedure of excited state dynamics implies that our simulations follow Ehrenfest dynamics, that is, the quantum states of coupled electron-ion motion are reduced to the classical ionic trajectories. Thus, our approach represents a mean-field theory of the mixed quantum-classical system, with forces on the ions averaged over many possible adiabatic electronic states induced by the ionic motion. This approximation works well for situations where a single path dominates in the reaction dynamics, for the initial stages of excited states before significant surface crossings take place, or for cases where the state-averaged behavior is of interest when many electron levels are involved as in condensed phases. However, the approach has limitations when the excited states involve multiple paths, especially when state-specific ionic trajectories are of interest.[25] In such cases, Ehrenfest dynamics fails as it describes the nuclear path by a single average point even when the nuclear wave function has broken up into many distinct parts. It also lacks a detailed balance for quantum electronic states.[26] We limit our studies to the former cases and especially look into the early stages of excited states. When there is branching, our approach can address issues related to the mechanisms leading to the branch or decay. For alternative strategies, when trajectories other than Ehrenfest dynamics are needed to model nonadiabatic processes, the reader is referred to methods which explicitly include electron transitions such as trajectory surface hopping.[27]

The rest of this paper is organized as follows. In Sec. II, we describe the methodology we propose for the real-time, local basis-set implementation of TDDFT. In Sec. III, we present and discuss results for some small molecules. Finally, concluding remarks are given in Sec. IV.

II. METHODOLOGY

A. TDKS equation for coupled electron-ion motion

The general time-dependent Schrödinger equation for the coupled electron-ion systems can be formally written as

$$i\hbar\frac{\partial\Psi(\{\mathbf{r}_j\},\{\mathbf{R}_J\},t)}{\partial t}=\mathcal{H}_{\mathrm{tot}}(\{\mathbf{r}_j\},\{\mathbf{R}_J\},t)\Psi(\{\mathbf{r}_j\},\{\mathbf{R}_J\},t), \quad (1)$$

where $\mathbf{r}_j$ and $\mathbf{R}_J$ denote the positions of the jth electron and Jth ion, respectively. $\mathcal{H}_{\mathrm{tot}}$ is the time-dependent Hamiltonian of the multicomponent system[28] given by

$$\mathcal{H}_{\mathrm{tot}}=-\sum_j\frac{\hbar^2}{2m}\nabla_j^2-\sum_J\frac{\hbar^2}{2M_J}\nabla_J^2+\frac{1}{2}\sum_{i\neq j}\frac{e^2}{|\mathbf{r}_i-\mathbf{r}_j|}+\frac{1}{2}\sum_{I\neq J}\frac{Z_IZ_J}{|\mathbf{R}_I-\mathbf{R}_J|}-\sum_{j,J}\frac{eZ_J}{|\mathbf{r}_j-\mathbf{R}_J|}+U_{\mathrm{ext}}(\{\mathbf{r}_j\},\{\mathbf{R}_J\},t). \quad (2)$$

And $\Psi(\{\mathbf{r}_j\},\{\mathbf{R}_J\},t)$ is the many-body wave function for the system. In this expression m and M_J denote the mass of electrons and of the Jth ion, Z_J denotes the ionic charge, and U_{ext} is the external potential. The Runge–Gross theorem[2] states that there exists a one-to-one mapping between the external potentials and the particle densities for a given initial many-body state $\Psi(\{\mathbf{r}_j\},\{\mathbf{R}_J\},t=0)$. In principle, this applies to both the electronic and ionic systems, so that the external potentials for the electrons and the ions are determined only by their respective densities,[29] ρ and ρ_J. The following TDKS equations can be derived:

$$i\hbar\frac{\partial\phi_j(\mathbf{r},t)}{\partial t}=\left(-\frac{\hbar^2}{2m}\nabla_{\mathbf{r}}^2+v_s[\rho](\mathbf{r},t)\right)\phi_j(\mathbf{r},t), \quad (3)$$

$$\rho(\mathbf{r},t)=\sum_j|\phi_j(\mathbf{r},t)|^2, \quad (4)$$

$$i\hbar\frac{\partial\psi_J(\mathbf{R},t)}{\partial t}=\left(-\frac{\hbar^2}{2M_J}\nabla_{\mathbf{R}}^2+V_s^J[\rho_J](\mathbf{R},t)\right)\psi_J(\mathbf{R},t), \quad (5)$$

$$\rho_J(\mathbf{R},t)=|\psi_J(\mathbf{R},t)|^2. \quad (6)$$

The single-particle KS potentials v_s and V_s^J contain terms such as the external potential (including the ionic potential for electrons and the electronic attraction potential for ions), the Hartree potential, and the exchange-correlation potential that depends only on the corresponding density. Note that in the above approximation the correlation interaction between the electronic density and the ionic density is not considered explicitly; in other words, the electronic and ionic subsystems are decoupled in the exchange-correlation functionals. The correlation between ions and electrons is important and has to be included if the intention is to obtain accurate ionic wave functions and ionic energy separations (vibration

energies), especially for protons.[30] However, as shown below, by invoking the Ehrenfest theorem and classical trajectories for ions, the absence of explicit ion-electron correlation leads to Born–Oppenheimer-type dynamics for ground-state simulations and correct vibration frequencies in both ground and excited states. This indicates that the correlation between ions and electrons is implicitly taken into account by Coulomb interactions and this implicit representation is adequate to give physically meaningful results. The explicit expressions for v_s and V_s^J are as follows:

$$v_s[\rho](\mathbf{r},t) = v_{\text{ext}}(\mathbf{r},t) - \sum_I \int \frac{Z_I \rho_I(\mathbf{R},t)}{|\mathbf{r}-\mathbf{R}|} d\mathbf{R} + \int \frac{\rho(\mathbf{r}',t)}{|\mathbf{r}-\mathbf{r}'|} d\mathbf{r}' + v_{\text{xc}}[\rho](\mathbf{r},t), \tag{7}$$

$$V_s^J[\rho_J](\mathbf{R},t) = V_{\text{ext}}^J(\mathbf{R},t) - Z_J \int \frac{\rho(\mathbf{r},t)}{|\mathbf{R}-\mathbf{r}|} d\mathbf{r} + Z_J \sum_I \int \frac{Z_I \rho_I(\mathbf{R}',t)}{|\mathbf{R}-\mathbf{R}'|} d\mathbf{R}' + V_{\text{xc}}^J[\rho_J](\mathbf{R},t). \tag{8}$$

It is convenient to treat the ionic subsystems classically because ions are much heavier than electrons, at least by three orders of magnitude. In doing this, we invoke the Ehrenfest theorem for the ionic TDKS equation. By defining the classic ionic path $\mathbf{R}_J^{\text{cl}}(t)$ and forces $\langle \mathbf{F}_J(t) \rangle$ as

$$\mathbf{R}_J^{\text{cl}}(t) = \langle \psi_J(\mathbf{R},t) | \hat{\mathbf{R}} | \psi_J(\mathbf{R},t) \rangle = \int \mathbf{R} \rho_J(\mathbf{R},t) d\mathbf{R}, \tag{9}$$

$$\langle \mathbf{F}_J(t) \rangle = -\langle \psi_J(\mathbf{R},t) | \nabla_{\mathbf{R}} V_s^J | \psi_J(\mathbf{R},t) \rangle = -\int \rho_J(\mathbf{R},t) \nabla_{\mathbf{R}} [V_s^J[\rho_J](\mathbf{R},t)] d\mathbf{R}, \tag{10}$$

we obtain

$$M_J \frac{d^2 \mathbf{R}_J^{\text{cl}}(t)}{dt^2} = \langle \mathbf{F}_J(t) \rangle, \tag{11}$$

which recovers Newton's second law of motion for the ionic degrees of freedom. If we ignore the negligible ion-ion exchange-correlation function and assume that the ionic density has a sharp distribution

$$\rho_J(\mathbf{R},t) = \delta(\mathbf{R} - \mathbf{R}_J^{\text{cl}}(t)), \tag{12}$$

we obtain the simpler coupled ion-electron equations,

$$M_J \frac{d^2 \mathbf{R}_J^{\text{cl}}(t)}{dt^2} = -\nabla_{\mathbf{R}_J^{\text{cl}}} \left[V_{\text{ext}}^J(\mathbf{R}_J^{\text{cl}},t) - \int \frac{Z_J \rho(\mathbf{r},t)}{|\mathbf{R}_J^{\text{cl}} - \mathbf{r}|} d\mathbf{r} + \sum_{I \neq J} \frac{Z_J Z_I}{|\mathbf{R}_J^{\text{cl}} - \mathbf{R}_I^{\text{cl}}|} \right], \tag{13}$$

$$i\hbar \frac{\partial \phi_j(\mathbf{r},t)}{\partial t} = \left[-\frac{\hbar^2}{2m} \nabla_{\mathbf{r}}^2 + v_{\text{ext}}(\mathbf{r},t) + \int \frac{\rho(\mathbf{r}',t)}{|\mathbf{r}-\mathbf{r}'|} d\mathbf{r}' - \sum_I \frac{Z_I}{|\mathbf{r}-\mathbf{R}_I^{\text{cl}}|} + v_{\text{xc}}[\rho](\mathbf{r},t) \right] \phi_j(\mathbf{r},t). \tag{14}$$

Equations (13) and (14) describe the time-dependent evolution of a coupled electron-ion system. The electronic subsystem is described within TDDFT, whose evolution is merely dependent on its density and the initial state with a total potential that includes a term representing the moving ions. The ionic subsystem, in turn, is described classically, evolving along the Newtonian trajectories with forces that include the effect of electrons by making use of the Ehrenfest theorem, and are determined by the electronic density corresponding to either the ground state or an excited state. Note that the above derivation does not involve the Born–Oppenheimer approximation because the evolution of the electronic and ionic subsystems is performed separately without finding the electronic ground state each time the ions are moved. Simulations beyond the classical Ehrenfest trajectories for the ions, using Eqs. (3)–(6) instead of Eq. (12), can be performed in principle, but are limited by the lack of reliable ion-ion and electron-ion correlation functionals and are not practical at present.

B. Numerical atomic orbitals

Our implementation of TDDFT involves describing electronic wave functions by a linear combination of atomic orbitals (LCAOs). The size of the LCAO basis is usually small, especially for the first-row elements which are predominant in the composition of biomolecules. This leads to matrix sizes in the LCAO representation considerably smaller than for other basis sets such as plane waves and real-space grids.[23] As a result, the TDDFT calculations can be done very efficiently.

Our scheme is based on the SIESTA code,[31] which is used to compute the initial wave functions and the Hamiltonian matrix for each time step. This is a general-purpose DFT code that uses a local basis which comprises a set of numerical atomic orbitals (NAOs), constructed from the eigenstates of the atomic pseudopotentials.[32,33] The NAOs are spatially confined, being strictly zero beyond a certain radius from the nucleus. In addition, the electron wave functions and density are projected onto a real-space grid in order to calculate the Hartree and exchange-correlation potentials and their matrix elements.

The use of confined NAOs is very important for the efficiency of the SIESTA code. By exploiting the explicit sparseness of the Hamiltonian and density matrices, the computational cost for the construction and storage of the Hamiltonian and the electronic density can be made to scale linearly with the number of atoms, in the limit of large systems. Therefore, a considerable effort has been devoted to obtaining orbital bases that meet the standards of accuracy of conventional first-principles calculations, while keeping their range as small as possible. A simple scheme for the genera-

tion of transferable bases that satisfy both requirements was presented in Refs. 34 and 35.

These bases have been successfully applied to study the ground-state properties of very different systems, ranging from insulators to metals, and from bulk to surfaces and nanostructures.[36] The approach was also shown to reproduce adequately the experimental optical absorption peaks in TDDFT calculations of biomolecules,[23,24] within a general accuracy of 0.2–0.3 eV, which is comparable to other approaches using more demanding basis sets such as real-space grids. For very diffusive excited states such as Rydberg states and atomic collision, the use of a local basis set will be inadequate and should be complemented with diffusive functions. As it is specially optimized to deal with large systems, a TDDFT simulation based on SIESTA with a local basis set represents an ideal tool for treating large nanoclusters and biomolecules.

C. Solving the TDKS equation

Efficient solution of the TDKS equations, as expressed in Eq. (14), is of particular interest because it is one of the two most time-consuming parts of the calculation, the other one being the computation of the time-dependent Hamiltonian. In the LCAO formalism, Eq. (14) takes the form (neglecting time derivatives of bases)[23]

$$i\hbar\frac{\partial \mathbf{c}}{\partial t} = \mathcal{S}^{-1}\mathcal{H}\mathbf{c}, \tag{15}$$

where $\mathcal{H}$ is the KS Hamiltonian, $\mathbf{c}$ is the column of coefficients of the local basis $\{\mu_i\}$, and $\mathcal{S}$ is the overlap matrix,

$$\phi_j = \sum_i c_i^{(j)}\mu_i, \mathcal{S}_{ij} = \langle \mu_i|\mu_j\rangle, \tag{16}$$

with the superscript index j of the coefficient c identifying the electronic KS state ϕ_j to which it belongs and the subscript index i identifying the basis element μ_i to which it corresponds; the total number of coefficients c (the length N_t of the vector $\mathbf{c}$) is equal to

$$N_t = \sum_{s=1}^{N_s} N_{\mathrm{at}}^s N_{\mathrm{bs}}^s,$$

where N_s is the number of species of atoms in the system, N_{at}^s is the number of atoms of species s, and N_{bs}^s is the number of basis functions corresponding to species s. The overlap matrix depends on the ionic configuration, so it has to be updated and inverted at each ionic step when the ions move. The formal solution of TDKS then becomes (in the following we omit both indices of c for simplicity)

$$\begin{aligned} c(t+\Delta t) &= \mathcal{U}(t+\Delta t,t)c(t) \\ &= \hat{T}\exp\left(-i\hbar\int_t^{t+\Delta t}\mathcal{S}^{-1}(t')\mathcal{H}(t')dt'\right)c(t) \end{aligned} \tag{17}$$

with $\hat{T}$ as the time ordering operator. If the time step Δt is small enough,

$$\mathcal{U}(t+\Delta t,t) = \exp[-i\hbar\mathcal{S}^{-1}(t)\mathcal{H}(t)\cdot\Delta t]. \tag{18}$$

We can approximate the above exponential to be the Crank–Nicholson operator[37,38]

$$c(t+\Delta t) = \frac{1-i\hbar\mathcal{S}^{-1}(t)\mathcal{H}(t)\Delta t/2}{1+i\hbar\mathcal{S}^{-1}(t)\mathcal{H}(t)\Delta t/2}\cdot c(t). \tag{19}$$

The advantages of this approximation are the following: First, it is unitary, preserving the orthonormality of propagating wave functions. Second, it is time reversal invariant, and conserves the total energy of the system satisfactorily, even with a relatively large time step. Third, it is easy to be implemented and fast in actual calculations. The stability can be further improved by using a higher order Crank–Nicholson operator at the cost of computation time, for example,

$$\begin{aligned} c(t+\Delta t) &= \frac{1-i\hbar\mathcal{S}^{-1}\mathcal{H}\Delta t/2-\frac{1}{2}(\hbar\mathcal{S}^{-1}\mathcal{H}\Delta t/2)^2+i\frac{1}{6}(\hbar\mathcal{S}^{-1}\mathcal{H}\Delta t/2)^3}{1+i\hbar\mathcal{S}^{-1}\mathcal{H}\Delta t/2-\frac{1}{2}(\hbar\mathcal{S}^{-1}\mathcal{H}\Delta t/2)^2-i\frac{1}{6}(\hbar\mathcal{S}^{-1}\mathcal{H}\Delta t/2)^3} \\ &\quad\cdot c(t). \end{aligned} \tag{20}$$

In this formulation of TDDFT, we do not have to calculate all the occupied and unoccupied molecular orbitals, unlike in perturbative methods. Only occupied states and those excited states which are (partially) occupied after excitation need to be included in the calculation: Their wave functions are propagated and their densities are added into the total electronic density after multiplying with the new occupancy number after excitation.

D. Molecular dynamics simulations

With the present scheme, we can perform *ab initio* molecular dynamics (MD) for coupled electron-ion systems. The ions are moved following Newtonian dynamics in the presence of the electrostatic field due to the electrons. The Verlet algorithm is employed to calculate the ionic velocities and positions at each time step. When the initial conditions are chosen, the electronic subsystem may populate any state, ground or excited, and is coupled nonadiabatically with the motion of the ions. During the simulation, the occupation of KS orbitals is fixed. Such an approach may have limitations when electron transitions are involved, but our goal in the present work is to simulate the initial stages of excited states before significant electron transitions take place and to determine when such transitions may occur. The population change can be invoked by calculating the nonadiabatic coupling in the surface hopping method or by estimating the transition probability using the Landau–Zener formula.[39] This framework can be used to study chemical reactions, photoinduced dynamics of molecules, or a combination of both (photoinduced chemical reactions).

The practical simulation of excited state molecular dynamics is performed in the flowchart shown in Fig. 1. At time $t=0$, a self-consistent diagonalization is performed for a given ionic configuration $\{R(0)\}$ at the initial temperature determined by the ionic velocities $\{v(0)\}$. The resulting KS eigenstates are $\{\phi_j(0)\}$, where j is the index of the occupied states. Electronic excitation is modeled by switching the

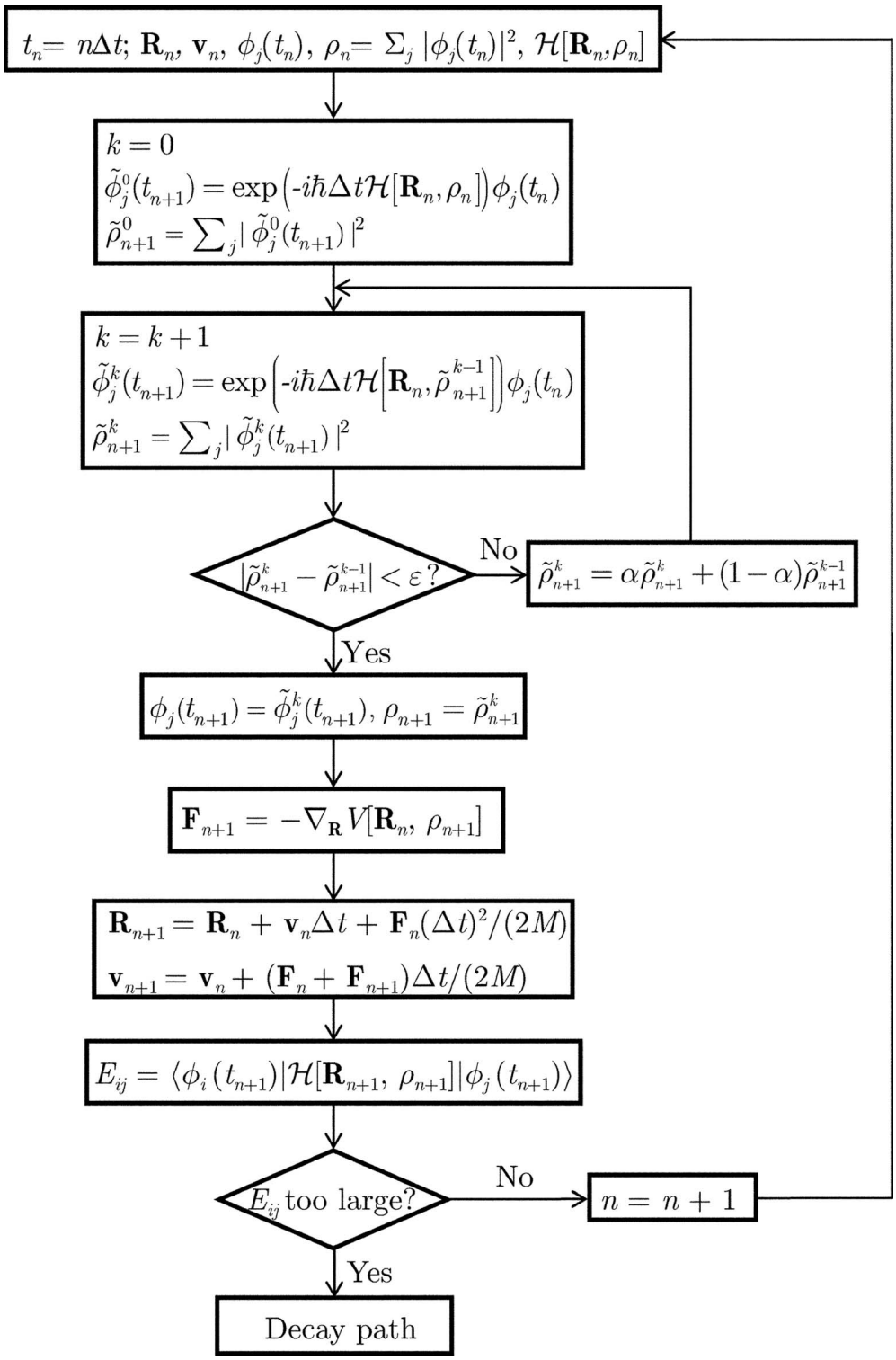

FIG. 1. Flowchart of the excited state MD simulation. The iterations over the index k describe the self-consistency loop. E_{ij} in the second rhombus box is the off-diagonal Hamiltonian matrix element ($i \neq j$).

occupation of the KS states involved in the excited state from that corresponding to the ground state. Note that the self-consistent electron density includes only contributions from an updated set of occupied states; for an excited state configuration this amounts to a constrained DFT calculation at $t=0$. In principle, partial occupation of several states is also possible. We note that in TDDFT the preparation of the initial electronic state is critical, especially for excitations that involve degenerate KS orbitals. The electron dynamics will depend sensitively on the initial wave functions and density. While the dependence of time evolution of the electronic system on the initial KS orbital occupancy is an important issue which we will address further in future work, the present simple treatment based on switching orbital occupancies represents a good approximation of the excited states introduced by photoexcitation.[18,29] In addition, the ex-

citation energy obtained by this approximation is reasonably close to that measured in experiment, as discussed in the examples.

At $t>0$, the time evolution of $\{\phi_j(t)\}$ is realized by multiplying the time propagator at the nth step ($t_n=n\Delta t$). Before the new wave function can be accepted, a self-consistent operation is performed,[16] as shown explicitly in Fig. 1. This process guarantees time reversal symmetry and is critical to the stability of the simulation for long times. We emphasize that the self-consistent loop here has nothing to do with self-consistency in the ground-state calculation because no diagonalization of the Hamiltonian matrix is performed. The new wave functions $\{\phi_j(t_{n+1})\}$ are *not* eigenstates of the updated Hamiltonian $\mathcal{H}(t_{n+1})$, but their density produces the same potential by which they are generated. A Pulay mixing scheme is used during this self-consistent calculation and only occupied KS states are needed for the time evolution as before.

Once the self-consistent potential is obtained, the forces acting on the ions can be calculated. In practice, this can be done through the Hellmann–Feynman theorem: The forces on ions introduced by the electron subsystem, that is, the second term in Eq. (13), can be written in the form

$$\sum_j \nabla_{\mathbf{R}}\langle\phi_j|\frac{Z}{|\mathbf{R}-r|}|\phi_j\rangle \approx \sum_j \langle\phi_j|\nabla_{\mathbf{R}}\frac{Z}{|\mathbf{R}-r|}|\phi_j\rangle. \tag{21}$$

The above equation is exact only if $\{\phi_j\}$ are the eigenstates of the KS Hamiltonian of the electron-ion system (the Hellmann–Feynman theorem). However, as described above, this is *not* the case in TDDFT for any given $t>0$. But, if the system does not deviate too much from its state at $t=0$ where exact diagonalization of the Hamiltonian matrix has been performed, the wave functions $\{\phi_j\}$ are close to the exact eigenfunctions of $\mathcal{H}$, and the approximation holds. To be precise, the Coulomb interaction between ions and electrons in Eqs. (13) and (21) should be replaced with the electronic Hamiltonian $\mathcal{H}$ when calculating the Hellmann–Feynman forces. The other two force terms, the electrostatic repulsion between ions and the external force, are trivial to calculate.

After evaluating all the force terms on each ion, we can then perform the classical MD simulation for the ionic motion. The new ionic positions $\{\mathbf{R}_{n+1}\}$ and velocities $\{\mathbf{v}_{n+1}\}$ at time $t_{n+1}=(n+1)\Delta t$ are calculated according to the velocity Verlet algorithm, as indicated in Fig. 1.

In order to assess the applicability of Hellmann–Feynman forces in the TDDFT-MD simulation outlined above, we monitor the off-diagonal Hamiltonian matrix elements

$$E_{ij}(t_n)=\langle\phi_i(t_n)|\mathcal{H}[\mathbf{R}_n,\rho_n]|\phi_j(t_n)\rangle. \tag{22}$$

A large value of E_{ij} $(i\neq j)$ comparable to typical energy separations $(E_{ii}-E_{jj})$ suggests high tendency of state mixing and high recombination probability between states i and j; it also indicates the failure of the nonadiabatic simulation when it becomes comparable to the typical separation between energy levels because the Hellmann–Feynman theorem fails. The time at which this failure occurs provides an estimate of the delay before the onset of nonradiative relaxation and of the decay lifetime in cases of prompt transitions.[40,41] Generally, the lifetime of excited states depends on both this delay (which we estimate here) and the nonadiabatic transition probability in cases where avoided surface crossings are traversed multiple times. The transition probability is a function of both the adiabatic energy separation and the nonadiabatic coupling, and is sensitive to the topography of potential energy surfaces around surface crossings.[42,43] Accurate potential energy surfaces for excited states and the nonadiatic couplings[44–47] between them can be calculated in linear response TDDFT (with the exception,[5] for example, of multiple-excited states). Nonadiabatic transition probabilities could also be analyzed using simple semiclassical models, such as the Landau–Zener formula for avoided crossings.[39] We elaborate on this type of analysis next.

The Landau–Zener theory is originally formulated to study the nonadiabatic transition at the linear crossing of two electronic states i and j, which provides a reasonable estimate of the transition probability in many cases.[39] The Landau–Zener transition probability is[39,48]

$$P=\exp\left(-\frac{\pi}{4}|\xi|\right), \tag{23}$$

where ξ is the Massey parameter

$$\xi=\frac{\Delta E}{\hbar\langle\varphi_i|\frac{d}{dt}|\varphi_j\rangle}. \tag{24}$$

Here ΔE is the energy separation between two adiabatic states φ_i and φ_i. For the application to the following examples, we choose only two states which are involved in the transition in our analysis, because usually only the off-diagonal matrix elements between them are significant, thus they constitute a complete active space in a sense similar to that in quantum chemistry. Therefore, $\Delta E=E_i'-E_j'$ (E_i' and E_j' being the adiabatic energy eigenvalues) can be calculated by a (2×2) matrix diagonalization

$$\begin{pmatrix}\cos\theta & \sin\theta\\ -\sin\theta & \cos\theta\end{pmatrix}\begin{pmatrix}E_{ii} & E_{ij}\\ E_{ij} & E_{jj}\end{pmatrix}\begin{pmatrix}\cos\theta & -\sin\theta\\ \sin\theta & \cos\theta\end{pmatrix}=\begin{pmatrix}E_i' & 0\\ 0 & E_j'\end{pmatrix}. \tag{25}$$

Here the mixing angle θ must satisfy

$$\tan 2\theta=\frac{2E_{ij}}{E_{ii}-E_{jj}}, \tag{26}$$

with

$$\begin{pmatrix}\varphi_i\\ \varphi_j\end{pmatrix}=\begin{pmatrix}\cos\theta & \sin\theta\\ -\sin\theta & \cos\theta\end{pmatrix}\begin{pmatrix}\phi_i\\ \phi_j\end{pmatrix}. \tag{27}$$

Following the derivation in Ref. 39, we have

$$\xi=\frac{\Delta E}{\hbar\dot{\theta}}. \tag{28}$$

Substituting Eq. (28) into Eq. (23) allows us to calculate the Landau–Zener transition probability between the two states in question in our excitation state dynamics.

In principle, both spin-polarized and spin-unpolarized calculations can be applied to the above scheme, so that the dynamics of both spin triplet excited states and spin singlet states can be studied. For simplicity, in all the following illustrative examples, we use the spin-unpolarized calculation only, amounting to taking account of spin singlet excitation states which are usually lower in energy than spin triplet states. Our approach is similar to the semiclassical electron-radiation-ion dynamics (SERID) method,[49,50] which simulates ion and electron dynamics following an applied laser pulse, except that the SERID method uses very limited atomic bases, a semiempirical Hamiltonian with parameters calculated from DFT, and an explicit radiation field.

III. APPLICATIONS

In order to demonstrate the potential of the method for realistic simulations, we give several examples of how it applies to small molecules. Note that the fact we are performing "nonadiabatic simulations" here for the systems of interest does not mean all the processes we investigated have a significant "nonadiabatic behavior." In fact, the processes we simulated either have negligible nonadiabatic effects (e.g., H_2 ground state) or stay at an initial stage of nonadiabatic process, before the nonadiabatic coupling grows large and the branching/surface hopping takes place. This is by choice since we are mostly interested in extracting estimate for the time scale in which nonadiabatic effects (such as nonradiative relaxation processes) take place.

A. Computational parameters

The parameters used in all the calculations are the following: We use Troullier–Martin pseudopotentials[51] and the adiabatic local density approximation for the exchange-correlation functional. An auxiliary real-space grid[52] equivalent to a plane-wave cutoff of 70 Ry is employed. The systems evolve typically with a time step of 24.19×10^{-3} fs, unless otherwise specified. The total energy is well conserved to within 10^{-5} eV/fs. The initial velocity of ions is assigned according to the equilibrium Boltzmann–Maxwell distribution at a given temperature.

We use a basis of double-zeta polarized orbitals. For C, this basis set includes 13 NAOs: two radial functions to represent the $2s$ states with confinement radii $r_s=5.12$ a.u. and two additional $2p$ shells plus a polarization[34] p shell with confinement radii $r_p=r_p^{\mathrm{Pol}}=6.25$ a.u. For every H atom, we have 5 NAOs: two radial shapes for the $1s$ orbital and a polarization s orbital with confinement radii $r_s=r_s^{\mathrm{Pol}}=6.05$ a.u. For the N atom, we have 13 orbitals: two $2s$ shells, two $2p$ shells, and a polarization p orbital with radii $r_s=4.50$ a.u. and $r_p=r_p^{\mathrm{Pol}}=5.50$ a.u., respectively. Finally, the number of orbitals for every O atom is also 13, with two $2s$ shells, two $2p$ shells, and a p polarization shell with confinement radii $r_s=3.93$ a.u. and $r_p=r_p^{\mathrm{Pol}}=4.93$ a.u., respectively. For the systems under study, it was found that inclusion of additional shells does not alter noticeably the results. The completeness of the basis is also evident from the fact that the f-sum rule for all small molecules is in the 96%–98% range.[24]

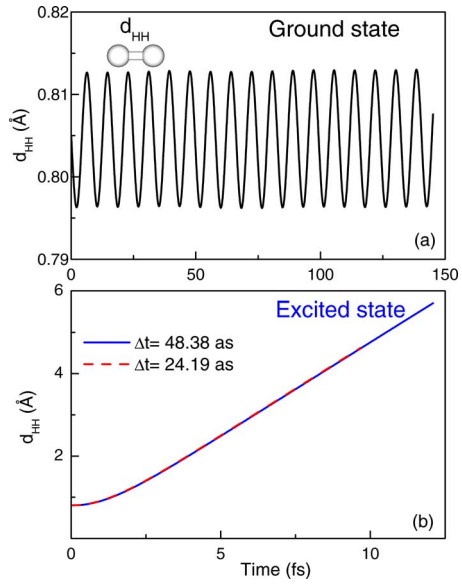

FIG. 2. (Color online) Nonadiabatic *ab initio* MD simulation of H_2: (a) ground state and (b) the first singlet excited state. The H–H bond length is plotted as a function of simulation time. Two different time steps are used in (b).

B. H_2 molecule

The simplest case we considered is the dynamic processes in the homopolar diatomic H_2 molecule, which in its ground state has two $1s$ electrons forming a σ-bonding state. To test the stability and accuracy of our proposed methodology, we first simulate the ground-state dynamics of H_2 without altering the occupancy of occupied and unoccupied states. Note that this is different from the usual so-called "*ab initio* MD" in literature because at each step we propagate electronic wave functions and ionic positions separately without diagonalization of the Hamiltonian matrix. The initial configuration is fully relaxed and an initial temperature of 30 K is imposed, with a timestep of 0.048 38 fs. The H–H bond length variation with time is shown in Fig. 2(a). The amplitude and periodicity of H–H stretch mode are nicely preserved without any apparent deterioration for a simulation time of 150 fs. The H–H stretch frequency obtained from the oscillation is 4069 cm^{-1}, in good agreement with the experimental value of 4155 cm^{-1}.

We study next the singlet excitation from the σ-bonding state to the antibonding σ^* state: at $t=0$, an electron is promoted from the highest occupied molecular orbital (HOMO) to the lowest unoccupied molecular orbital (LUMO). Then the excited system evolves according to the TDDFT-MD scheme described above. The half occupation of the antibonding σ^* LUMO state results in large repulsive force between the two H atoms, which drives them apart and splits the H_2 molecule. The H–H splitting trajectory is plotted for 10 fs in Fig. 2(b). During this process, the total energy of the system, which includes the potential energy and the ionic kinetic energy, is well conserved while the potential energy decreases [Fig. 3(a)].

We also monitor the energy levels $E_i\equiv E_{ii}$, that is, the diagonal matrix elements of the Hamiltonian as defined in Eq. (22), as a function of time, shown in Fig. 3(a). We adopt

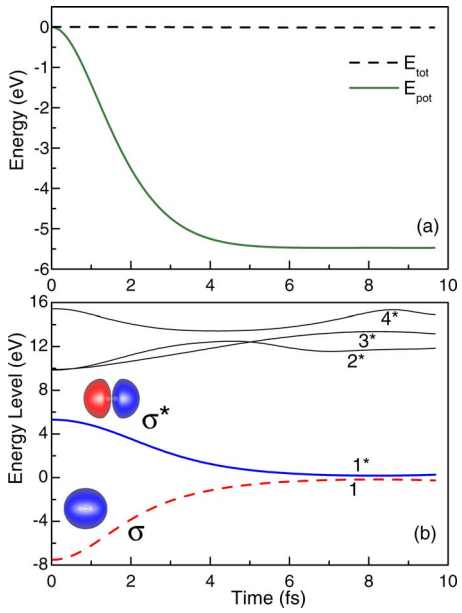

FIG. 3. (Color online) (a) Total energy and potential energy evolution of the H_2 singlet excited state. (b) Evolution of the individual energy levels. An electron is promoted from the σ to the σ^* state (wave functions shown) at time $t=0$; state numbering is explained in the text.

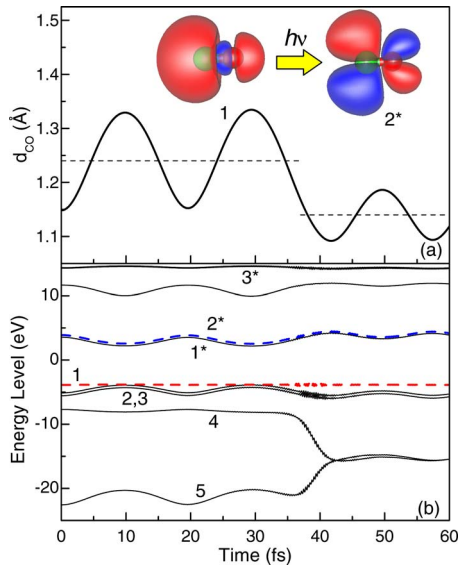

FIG. 4. (Color online) (a) CO bond length variation as a function of time after excitation from the HOMO to one of the two LUMOs. Corresponding wave functions are shown. Horizontal dashed lines show the average bond lengths at 1.24 and 1.14 Å. (b) Evolution of the corresponding molecular states. Dashed lines indicate the states where the excitation (switch of occupancy) is involved.

here and in the following examples the notation that occupied levels in the ground state of the molecule are labeled $1,2,\ldots$, counting from the HOMO toward lower energy, and unoccupied states are labeled $1^*,2^*,\ldots$, counting from the LUMO toward higher energy; for all the plots of E_i values, the Fermi level is set to zero. The time evolution of levels in Fig. 3(b) clearly shows the tendency that the two σ and σ^* states approach each other and become degenerate as the molecule dissociates. From the exponential decay of the eigenvalues, a lifetime of 3 fs can be estimated. We note that E_i is only the approximate energy levels because $|\phi_i(t)\rangle$ is not the real eigenstate of $\mathcal{H}(t)$. The off-diagonal matrix elements are very small (<0.05 eV) and give zero transition probability during the simulation. The two time steps of 0.048 38 and 0.024 19 fs we used give identical results, indicating the efficiency of our scheme: Relatively large time steps can be used that still maintain the numerical stability of the diabatic simulations.

C. CO molecule

A slightly more complex case is the heteropolar diatomic CO molecule. At $t=0$ (i.e., the Franck–Condon point), we excite a CO molecule by promoting an electron from the HOMO to one of the two LUMOs, which are degenerate in the ground state, forming an $A\ ^1\Pi$ excited state. These orbitals correspond to the $2p_z$ bonding state and the $2p_{x,y}$ hybrid states with z lying along the C–O axis [Fig. 4(a)]. For simplicity, we take CO to be in its ground-state configuration (calculated bond length 1.15 Å compared to the experimental value[53] of 1.13 Å) and zero temperature before excitation. We monitor the excited state trajectory in Fig. 4(a): The CO bond length is enlarged and oscillates around an equilibrium distance of 1.24 Å for the first 40 fs with a frequency of 1597 cm^{-1}. The corresponding experimental values are 1.24 Å and 1518 cm^{-1} for the CO $A\ ^1\Pi$ excited state,[53] in very good agreement with our results. The experimental excitation energy of 8.07 eV (Ref. 53) is also close to our calculated value of 7.76 eV. After $t=40$ fs, the system reaches a new state, where the CO bond length is decreased to ~1.14 Å. By monitoring the time evolution of the energy levels, we identified that this process is associated with the mixing of the two lowest energy states [Fig. 4(b)]. This is further confirmed by the off-diagonal matrix elements plot in Fig. 5(a). The E_{ij} value between these two states increases from 0 to ~5 eV during $t=30-40$ fs, indicating significant mixing between the two states. It also introduces a large difference in the diabatic and adiabatic energy separations between the two states. The mixing angle θ is shown in Fig. 5(b). It increases from zero to around 45°, with the largest time derivative occurring at $t=39$ fs [Fig. 5(c)]. At this time the adiabatic energy separation is still large, so that the calculated Landau–Zener transition probability is essentially zero. In this particular case, the mixing of states 4 and 5 has no physical consequences since both states are fully occupied, both before and after the transition.

D. O_3 molecule

A more complex system is the triatomic ozone molecule, which can be excited by ultraviolet (UV) light, a process related to the protective role of the ozone layer in the outer atmosphere and the greenhouse effect and air pollution at ground level.[54,55] The excited state potential energy surfaces have been extensively investigated,[55] and several important nonadiabatic transitions between different surfaces around conical intersections have been identified.[55,56] Here we focus on simple illustrations of possible photodissociation dynamics of O_3. In our calculation, we first conduct the ground-state MD of an O_3 molecule at 300 K for 100 fs (for $t<0$),

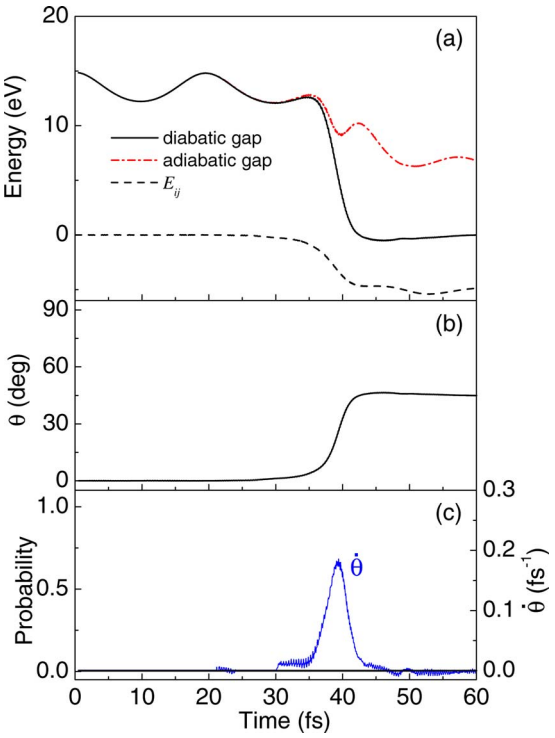

FIG. 5. (Color online) (a) The evolution of the off-diagonal Hamiltonian matrix element between states 4 and 5 in the CO molecule as a function of time after excitation. The diabatic and adiabatic energy gaps between the two states are also shown. (b) The mixing angle (θ) as a function of time. (c) The time derivative of the mixing angle ($\dot{\theta}$) and the Landau–Zener transition probability for the mixing of states 4 and 5.

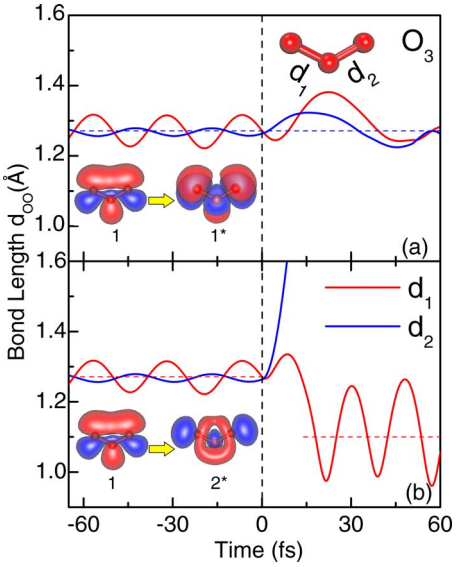

FIG. 6. (Color online) Variation of the two O–O bond lengths in an O_3 molecule from ground-state MD simulation (for $t<0$) and that from excited state simulation ($t>0$). Excitation takes place at $t=0$, when an electron is promoted: (a) from the HOMO to the LUMO and (b) from the HOMO to the LUMO+1. The geometry of the O_3 molecule and corresponding wave functions are shown in the insets. Horizontal dashed lines indicate average bond lengths at 1.27 and 1.10 Å.

then we excite an electron from the HOMO (π) to either the LUMO (π^*) or the LUMO+1 (σ^*) state at $t=0$ (wave functions are shown in Fig. 6). We find that the first process, which requires a photon of energy of 2.0 eV (620 nm), does not lead to O_3 dissociation in a short time. On the other hand, the second process involving a UV photon of energy of 8.4 eV (148 nm) leads to immediate O_3 dissociation into an isolated O and an O_2 molecule. The equilibrium O–O distance in the photoreaction product O_2 fragment is 1.10 Å, indicating a charged final state: The O–O distance is 1.22 Å in O_2, 1.15 Å in O_2^+, and 1.08 Å in O_2^{2+}, respectively. By analyzing the charge density, we find that the O_2 fragment has ~0.4 electrons missing so it is charged with a net charge of +0.4. Its bond length is similar to that of the ground-state O_2^{2+} molecule. This result is consistent with experiment.[54] The processes are shown in Fig. 6.

E. Indolequinone-methide

All of the above examples concerned very small molecules containing two or three atoms. As we pointed out earlier, because the biggest advantage of our real-time, local basis-set implementation of TDDFT-MD is its efficiency, targeted to simulation of big biomolecules and nanoclusters, we give here at least one example of a medium-sized molecule relevant to biological systems, the 5,6-dihydroxyindolequinone (referred to as DHI).

A DHI molecule comprises of two conjugate aromatic rings with a total number of 16 atoms, and is appended with O or OH groups on the six-membered ring. We have chosen to study the methide form of the molecule (indolequinone-methide or MQ), whose structure is shown in Fig. 7(a) (inset). This molecule and its tautomeric and oxidized forms constitute the main components of melanin pigments, which exist widely in animals, plants, and microorganism for the purpose of camouflage and photoprotection from UV exposure.[57] Understanding its molecular relaxation processes under light illumination is therefore very important.

Figures 7(b) and 7(c) show the time evolution of the total energy, the potential energy, and the energy levels of MQ after HOMO-LUMO excitation at time $t=0$ with an initial temperature of 0 K. We find that the total energy is well conserved for a duration of 120 fs, with an energy drift of $<1\times10^{-5}$ eV/fs and energy fluctuations of 2–5 meV. The potential energy quickly decreases from zero and then fluctuates around −0.25 eV with a periodicity of ~20 fs. After excitation the potential energy never returns to its initial value. This indicates that the photon energy is transferred into ionic kinetic energy (heat) within 10 fs, which is possibly related to ultrafast photoenergy conversion in melanin. The Fourier transform of the ionic velocity autocorrelation function gives the vibrational spectrum of the molecule after excitation, which is shown in Fig. 7(a). The main peaks are located at 3135, 1567, 1003 cm^{-1}, corresponding to C–H stretch, C–C and C–N stretch, and ring deformation modes, respectively. Vibrations at 1400–1600 cm^{-1} and ~980 cm^{-1} are experimentally observed in natural Sepia melanin.[58] We conclude from this analysis that the photon energy dissipates into these channels very efficiently after excitation. This analysis will be extended to similar processes in protomolecule structures, consisting of several DHI units, to elucidate the importance of this relaxation mechanism in the photoprotection function of melanin.

The off-diagonal matrix element and the corresponding

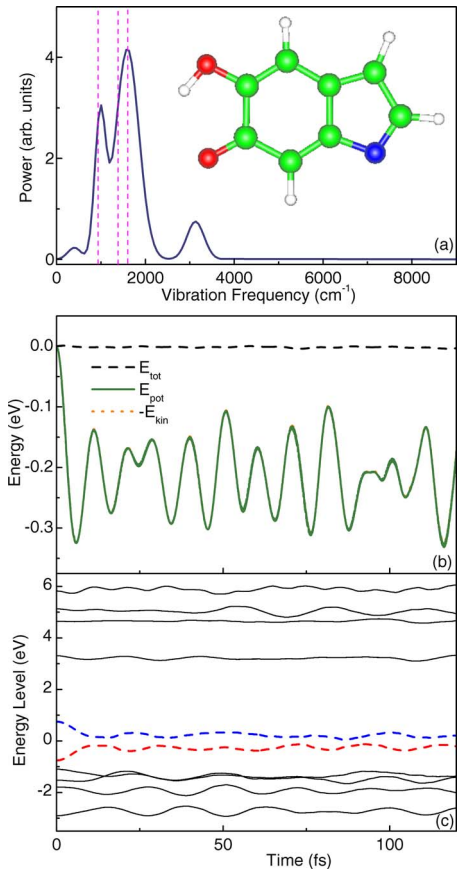

FIG. 7. (Color online) (a) Vibrational spectrum from excited state MD simulations of MQ molecule. The spectrum was obtained by Fourier transform of the velocity-velocity autocorrelation function, and fitted with three Gaussian peaks with a width of 500 cm^{-1}. Vertical dashed lines indicate the main frequencies from experiment. The inset is the atomic geometry of the molecule. (b) Evolution of the total energy (dashed line), potential energy (solid line), and kinetic energy of ions (with an opposite sign, dotted line) for the first excited state of MQ (HOMO to LUMO transition). (c) Evolution of the energy levels during the simulation. Dashed lines indicate the states involved in the excitation.

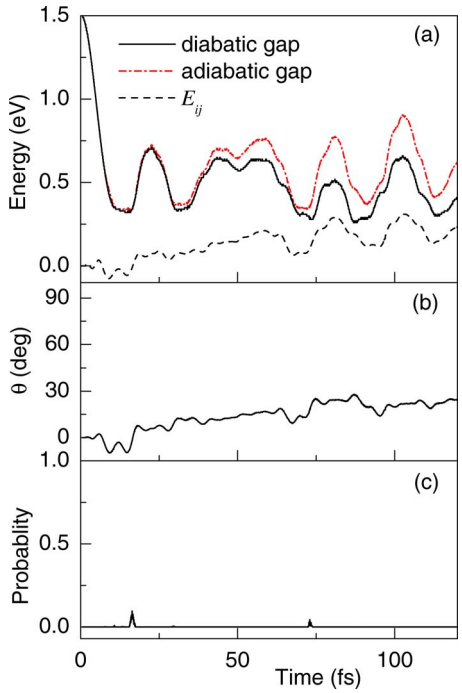

FIG. 8. (Color online) (a) Time evolution of the off-diagonal Hamiltonian matrix element between states 1 (HOMO) and 1* (LUMO), and the diabatic and adiabatic energy gaps in the first excited state of MQ. (b) The mixing angle θ and (c) the Landau–Zener transition probability between states 1 and 1* as a function of time upon excitation.

diabatic and adiabatic energy gaps between state 1 and 1* are shown in Fig. 8(a). Initially, the diabatic energy gap shows small deviation from the adiabatic one up to $t=50$ fs. As the off-diagonal matrix element grows bigger than ~0.25 eV, the difference between diabatic and adiabatic gaps become larger. The mixing angle θ generally follows the trend of E_{ij}, modulated by the diabatic gap, shown in Fig. 8(b), from its definition in Eq. (26). The Landau–Zener decay probability shown in Fig. 8(c) is small, less than 10% throughout the simulation ($t \leq 120$ fs), with two peaks located around $t=16$ and 73 fs. They correspond to the most abrupt changes in the angle θ, or the largest time derivative $\dot{\theta}$, and small adiabatic energy gaps as in Eqs. (23) and (28). This analysis indicates a fairly small transition probability from state 1* to 1 during the simulation lasting for 120 fs.

IV. CONCLUSION

In conclusion, we have proposed using a local basis set and real-time propagation of KS wave functions to simulate nonadiabatic electron-ion processes, especially the excited state dynamics of biomolecules and other nanostructures, in the framework of coupled TDDFT-MD simulations. This approach uses a small number of basis functions while maintaining high accuracy, thereby reducing significantly the memory requirements and the computation time compared to commonly used plane-wave and real-space grid bases.

In order to provide concrete evidence for these claims, we have repeated the calculations reported above with a standard real-space code and compared computer time and memory requirements to our method. Figure 9 summarizes the computer time consumed and memory used during the TDDFT-MD simulations of electron-ion dynamics in the systems we studied with our method. The pyrazine molecule is also included for the comparison. Overall the time for a simulation lasting for 1 fs and the memory scales approxi-

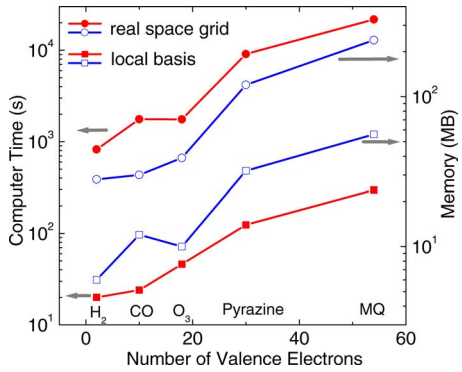

FIG. 9. (Color online) Computer time (filled symbols) for the simulation of 1 fs electron-ion dynamics and the memory required (empty symbols), plotted as a function of the number of valence electrons, using real-space grid [circles, OCTOPUS package (Ref. 15)] or a local basis set (squares, present method).

mately exponentially with the number of valence electrons in the molecule, which are 2, 8, 18, 39 and 54 for H_2, CO, O_3, pyrazine, and MQ, respectively. Compared with real-space grid methods that are commonly used in literature, both the computer time and memory requirements are greatly reduced. The comparison calculations based on a real-space grid were performed with the OCTOPUS package,[15] using a sphere box with radii of 4 Å for H_2, CO, O_3, 6 Å for pyrazine and 7 Å for MQ, a uniform spacing of 0.2 Å, and a time step of $0.658\ 212\ 20 \times 10^{-3}$ fs. The nearly two orders of magnitude decrease in computer time obtained by our method is mainly a result of the larger time step we use while still maintaining the conservation of total energy. The use of the local basis set, which is much smaller in size than a real-space grid, contributes greatly to the stability of the system's time evolution, the enhanced speed, and the reduced memory by about a factor of 4.

Parallelization over molecular states and order-N scaling performance are also natural extensions of the method due to the use of strictly confined NAOs. Only occupied states need to be calculated and nonlinear response is included by default. Our TDDFT-MD scheme has been successfully implemented within a well established *ab initio* package for ground-state DFT calculations. The application to excited states of small and medium-sized molecules reveals interesting characteristics of excited states, such as the excitation energy, vibrational frequencies, photodissociation pathways, and the decaying lifetime, all in good agreement with available experiments.

Like any method in practice, the present form of TDDFT-MD simulations also has its own limitations. First, the Ehrenfest theorem is employed when reducing the quantum states of coupled electron-ion motion to the classical ionic trajectories. As such, it represents a mean-field theory of the mixed quantum-classical system, with forces on the ions averaged over many possible nonadiabatic electronic states induced by the ionic motion. This approximation works well in many real cases but may fail when it becomes important to monitor different paths for different electronic states, especially when interested in state-specific ionic trajectories.[25] Alternative strategies going beyond Ehrenfest trajectories to model nonadiabatic processes have been developed recently, such as trajectory surface hopping,[11,17,27] nuclear wavepacket propagation,[59,60] full multiple spawning,[61,62] Wigner–Liouville formulation[63] and linearized path integral approaches.[64] Some of above schemes are coupled to first-principles TDDFT calculations[11,17] or quantum chemistry methods including CASSCF or CASPT2 (for instance, the *ab initio* multiple spawning method[62,65]) to allow direct simulations of excited state dynamics. Second, in some cases of chemical reactions and excited states, nonadiabatic wave functions are extremely diffusive and cannot be well represented by localized atomic orbitals. This is particularly relevant in high-energy atom collisions or scattering processes, where even free electrons can be generated. In such cases, the local basis needs to be complemented by nonlocal functions or fictitious atoms in order to describe appropriately the excited states. Despite these limitations, we believe that our method will perform well in a wide range of applications to photoexcitations and ultrafast chemical reactions, as suggested by the encouraging tests on the simple examples presented here. Calculations for more complex systems involving molecules with up to 80 atoms are currently under way and will be reported elsewhere.

ACKNOWLEDGMENTS

We are indebted to Dr. Sara Bonella for a careful reading of the manuscript and useful comments. This work was supported in part by DOE CMSN Grant DE-FG02–05ER46226 and the Harvard University Center for the Environment.

[1] P. Hohenberg and W. Kohn, Phys. Rev. **136**, B864 (1964); W. Kohn and L. Sham, *ibid.* **140**, A1133 (1965).
[2] E. Runge and E. K. U. Gross, Phys. Rev. Lett. **52**, 997 (1984).
[3] K. Burke, J. Werschnik, and E. K. U. Gross, J. Chem. Phys. **123**, 062206 (2005).
[4] F. Furche and K. Burke, in *Annual Reports in Computational Chemistry*, edited by D. Spellmeyer (Elsevier, Amsterdam, 2005), Vol. 1, pp. 19–30.
[5] B. G. Levine, C. Ko, J. Quenneville, and T. J. Martinez, Mol. Phys. **104**, 1039 (2006).
[6] M. E. Casida, C. Jamorski, K. C. Casida, and D. R. Salahub, J. Chem. Phys. **108**, 4439 (1998).
[7] S. I. Chu, J. Chem. Phys. **123**, 062207 (2005).
[8] Y. Zhao and D. G. Truhlar, J. Phys. Chem. A **110**, 13126 (2006).
[9] C. Hu, O. Sugino, and Y. Miyamoto, Phys. Rev. A **74**, 032508 (2006).
[10] M. E. Casida, in *Recent Developments and Applications in Density Functional Theory*, edited by J. M. Seminario (Elsevier, Amsterdam, 1996).
[11] E. Tapavicza, I. Tavernelli, and U. Rothlisberger, Phys. Rev. Lett. **98**, 023001 (2007).
[12] J. Theilhaber, Phys. Rev. B **46**, 12990 (1992).
[13] K. Yabana and G. F. Bertsch, Phys. Rev. B **54**, 4484 (1996).
[14] K. Yabana, T. Nakatsukasa, J. I. Iwata, and G. F. Bertsch, Phys. Status Solidi B **243**, 1121 (2006).
[15] A. Castro, H. Appel, M. Oliveira, C. A. Rozzi, X. Andrade, F. Lorenzen, M. A. L. Marques, E. K. U. Gross, and A. Rubio, Phys. Status Solidi B **243**, 2465 (2006).
[16] O. Sugino and Y. Miyamoto, Phys. Rev. B **59**, 2579 (1999).
[17] C. F. Craig, W. R. Duncan, and O. V. Prezhdo, Phys. Rev. Lett. **95**, 163001 (2005).
[18] I. Tavernelli, U. F. Rohrig, and U. Rothlisberger, Mol. Phys. **103**, 963 (2005).
[19] I. Tavernelli, Phys. Rev. B **73**, 094204 (2006).
[20] C. M. Isborn, X. Li, and J. C. Tully, J. Chem. Phys. **126**, 134307 (2007).
[21] I. Vasiliev, S. Ogut, and J. R. Chelikowsky, Phys. Rev. Lett. **82**, 1919 (1999).
[22] A. Castro, M. A. L. Marques, J. A. Alonso, G. F. Bertsch, and A. Rubio, Eur. Phys. J. D **28**, 211 (2004).
[23] A. Tsolakidis, D. Sanchez-Portal, and R. M. Martin, Phys. Rev. B **66**, 235416 (2002).
[24] A. Tsolakidis and E. Kaxiras, J. Phys. Chem. A **109**, 2373 (2005).
[25] M. Hack and D. Truhlar, J. Phys. Chem. A **104**, 7917 (2000).
[26] P. V. Parandekar and J. C. Tully, J. Chem. Theory Comput. **2**, 229 (2006).
[27] J. C. Tully, Faraday Discuss. **110**, 407 (1998).
[28] T. Kreibich and E. K. U. Gross, Phys. Rev. Lett. **86**, 2984 (2001).
[29] Y. Tateyama, N. Oyama, T. Ohno, and Y. Miyamoto, J. Chem. Phys. **124**, 124507 (2006).
[30] C. Swalina, M. V. Pak, A. Chakraborty, and S. Hammes-Schiffer, J. Phys. Chem. A **110**, 9983 (2006).
[31] D. Sanchez-Portal, P. Ordejon, E. Artacho, and J. M. Soler, Int. J. Quantum Chem. **65**, 453 (1997).
[32] O. F. Sankey and D. J. Niklewski, Phys. Rev. B **40**, 3979 (1989).
[33] D. Sanchez-Portal, E. Artacho, and J. M. Soler, J. Phys.: Condens. Matter **8**, 3859 (1996).
[34] E. Artacho, D. Sanchez-Portal, P. Ordejon, A. Garcia, and J. M. Soler, Phys. Status Solidi B **215**, 809 (1999).
[35] J. Junquera, O. Paz, D. Sanchez-Portal, and E. Artacho, Phys. Rev. B **64**, 235111 (2001).
[36] P. Ordejon, Phys. Status Solidi B **217**, 335 (2000).
[37] R. S. Varga, *Matrix Interative Analysis* (Prentice-Hall, Englewood Cliffs,

NJ, 1962), p. 263.
[38] A. Castro, M. A. L. Marques, and A. Rubio, J. Chem. Phys. **121**, 3425 (2004).
[39] M. Desouter-Lecomte and J. C. Lorquet, J. Chem. Phys. **71**, 4391 (1979).
[40] Y. Miyamoto and O. Sugino, Phys. Rev. B **62**, 2039 (2000).
[41] Y. Miyamoto, Phys. Status Solidi A **204**, 1925 (2007).
[42] D. R. Yarkony, J. Chem. Phys. **114**, 2601 (2001).
[43] M. Ben-Nun, F. Molnar, K. Schulten, and T. J. Martinez, Proc. Natl. Acad. Sci. U.S.A. **99**, 1769 (2002).
[44] Y. Chernyak and S. Mukamel, J. Chem. Phys. **112**, 3572 (2000).
[45] R. Baer, Chem. Phys. Lett. **364**, 75 (2002).
[46] C. Hu, H. Hirai, and O. Sugino, J. Chem. Phys. **127**, 064103 (2007).
[47] C. Hu, H. Hirai, and O. Sugino, J. Chem. Phys. **128**, 154111 (2008).
[48] L. M. Frutos, T. Andruniow, F. Santoro, N. Ferre, and M. Olivucci, Proc. Natl. Acad. Sci. U.S.A. **104**, 7764 (2007).
[49] Y. Dou, B. R. Torralva, and R. E. Allen, J. Mod. Opt. **50**, 2615 (2003).
[50] Y. Dou, Y. Lei, A. Li, Z. Wen, B. R. Torralva, G. V. Lo, and R. E. Allen, J. Phys. Chem. A **111**, 1133 (2007).
[51] N. Troullier and J. L. Martins, Phys. Rev. B **43**, 1993 (1991).
[52] D. Sánchez-Portal, P. Ordejón, E. Artacho, and J. M. Soler, Int. J. Quantum Chem. **65**, 453 (1997).
[53] *NIST Chemistry WebBook*, NIST Standard Reference Database No. 69, edited by P. J. Linstrom and W. G. Mallard (National Institute of Standards and Technology, Gaithersburg, MD, 2005); http://webbook.nist.gov
[54] Y. Matsumi and M. Kawasaki, Chem. Rev. (Washington, D.C.) **103**, 4767 (2003).
[55] S. Y. Grebenshchikov, Z. W. Qu, H. Zhu, and R. Schinke, Phys. Chem. Chem. Phys. **9**, 2044 (2007).
[56] S. Xantheas, S. T. Elbert, and K. Ruedenberg, J. Chem. Phys. **93**, 7519 (1990).
[57] E. Kaxiras, A. Tsolakidis, G. Zonios, and S. Meng, Phys. Rev. Lett. **97**, 218102 (2006).
[58] A. Samokhvalov, Y. Liu, and J. D. Simon, Photochem. Photobiol. **80**, 84 (2004).
[59] G. Ashkenazi, R. Kosloff, S. Ruhman, and H. Tal-Ezer, J. Chem. Phys. **103**, 10005 (1995).
[60] G. A. Worth, H. Patricia, and M. A. Robb, J. Phys. Chem. A **107**, 621 (2003).
[61] M. Ben-Nun and T. J. Martinez, J. Chem. Phys. **108**, 7244 (1998).
[62] M. Ben-Nun and T. J. Martinez, Adv. Chem. Phys. **121**, 439 (2002).
[63] G. Stock and M. Thoss, Phys. Rev. Lett. **78**, 578 (1997).
[64] S. Bonella and D. F. Coker, J. Chem. Phys. **122**, 194102 (2005).
[65] B. G. Levine and T. J. Martinez, Annu. Rev. Phys. Chem. **58**, 613 (2007).